Editors' Suggestion

Deep macroscopic pure-optical potential for laser cooling and trapping of neutral atoms

O. N. Prudnikov,[1,2,*] R. Ya. Ilenkov,[1,2] A. V. Taichenachev,[1,2] V. I. Yudin,[1,2,3] and S. N. Bagaev[1]
[1]*Institute of Laser Physics, 630090, Novosibirsk, Russia*
[2]*Novosibirsk State University, 630090, Novosibirsk, Russia*
[3]*Novosibirsk State Technical University, 630073, Novosibirsk, Russia*

(Received 23 June 2023; accepted 14 September 2023; published 9 October 2023)

We show the possibility of implementing a deep dissipative optical lattice for neutral atoms with a macroscopic period. The depth of the lattice can reach magnitudes comparable to the depth of the magnetooptical traps (MOT), while the presence of dissipative friction forces allows for the trapping and cooling of atoms. The area of localization of trapped atoms reaches submillimeter size, and the number of atoms is comparable to the number trapped in MOT. As an example, we study lithium atoms for which the macroscopic period of the lattice $\Lambda = 1.5$ cm. Such deep optical lattices with a macroscopic period open up the possibility for developing effective methods for cooling and trapping neutral atoms without the use of magnetic field as an alternative to MOT. This is important for developing compact systems based on cold atoms.

DOI: 10.1103/PhysRevA.108.043107

I. INTRODUCTION

Magnetooptical traps (MOT) are the basic instruments for laser cooling and trapping of neutral atoms [1,2]. The operation of MOT is based on a combination of dissipative forces of spontaneous light pressure and a deep macroscopic potential (of the order of several K) in a spatially nonuniform magnetic field. Cold atoms obtained in MOT have a wide range of applications, including the development of quantum sensors based on matter wave interference [3], in laser metrology for developments of ultra-precise frequency standards (atomic clocks) [4–7], and others. However, in many cases the fast turn-off of the magnetic field used in MOT and the precise control over the residual magnetic field are required, which may be technically difficult to realize. Therefore, the development of alternative methods of primary laser cooling and trapping of neutral atoms without using a magnetic field is an important direction in creating compact and mobile ultra-precision devices based on cold atoms.

It is well known that optical lattices allow for atom trapping without a magnetic field. Dissipative and nondissipative optical lattices are distinguished [2,8,9]. The regime of dissipative lattices [2,9–16], which combines atom trapping and laser cooling, is realized for small detunings, when the light-field frequency is close to the atom transition resonance with natural linewidth γ. However, since the frequency is chosen close to the atomic transition and the intensities of light waves required for deep cooling should be small, the depth of the dissipative lattice is usually small and comparable to the temperature of Doppler or sub-Doppler cooling. The absence of a deep macroscopic potential does not allow the use of such lattices for efficient primary laser cooling and trapping. Nondissipative deep optical lattices are created by intense light waves with a sufficiently large detuning. Their depth is determined by the technical capabilities of laser systems and can reach hundreds of microkelvin [2,4,17]. However, dissipative laser cooling mechanisms are negligible here, which requires the use of MOT to load atoms into them.

The use of bichromatic waves opens up new possibilities to form a deep dissipative potential of macroscopic scale. The first theoretical studies of atomic kinetics in the presence of two monochromatic fields were done in [18,19], where the effect of rectification of the dipole force was demonstrated. In such fields the atom acquires momentum $\Delta p = 2\hbar k$ due to induced absorption of photons of one of the counterpropagating waves and induced emission into the opposite wave. Since the rate of induced processes is not directly related to the line width γ, the force on the atom can significantly exceed the spontaneous light pressure force from a single wave, which can be used for effective control of atomic beams [20–23].

Moreover, in the bichromatic field, the force averaged over the wavelength is not equal to zero, making it possible to create a deep optical potential with a macroscopic period $\Lambda = \pi/\Delta k$, determined by the spatial beating of the two frequency components (Δk is difference in wave vectors). In this case, the parameters of the light field can be chosen so that the dissipative mechanisms of laser cooling lead to cooling and trapping of the atoms in the area of minimum of macroscopic potential [24,25]. However, because both field frequencys are resonant with the same optical transition, the difference in wave vectors is extremely small and Λ is very large. For example, for a frequency difference of 10 to 100 MHz is required for near-resonant interaction and the macroscopic period is about 1 to 10 meters. In such fields, the curvature in the minimum of the macroscopic potential ($\propto \Delta k/k$) is small and does not allow to reach a distinct localization of atoms inside cell of centimeter size since the spatial phase difference of the fields at such scales is practically unchanged.

*oleg.nsu@gmail.com

In this work, to reduce the period of the macroscopic potential in a bichromatic field and increase its curvature, we propose to use light waves, which are resonant to different transitions between fine and hyperfine components of atomic levels. As an example, we investigate lithium atoms, for which the fine splitting of the $^2P_{3/2}$ and $^2P_{1/2}$ levels is about 10 GHz, determining the macroscopic lattice period of $\Lambda = 1.5$ cm. In this case, each field component is near-resonant to the D_1 and D_2 lines, which leads to significant dipole forces and allows for the realization of a deep optical potential with a macroscopic period even in the low-intensity field. The presence of dissipative effects in such an optical lattice leads to laser cooling and trapping of neutral atoms with a submillimeter localization area near the minimum of the macroscopic potential. The results of our theoretical analysis show that the depth of the macroscopic potential is comparable to the depth of the magnetooptical trap (approximately 1 K in temperature units or more), and laser cooling temperatures can reach sub-Doppler values. These studies open up the possibility of implementing deep dissipative optical traps for neutral atoms as an alternative to MOT.

II. KINETICS OF LITHIUM ATOMS IN A RESONANT BICHROMATIC FIELD

In this section, we describe the kinetics of lithium atoms in a bichromatic light field with frequencies ω_1 and ω_2

$$\mathbf{E}(\mathbf{r},t) = \mathrm{Re}\{\mathbf{E}^{(1)}(\mathbf{r})e^{-i\omega_1 t} + \mathbf{E}^{(2)}(\mathbf{r})e^{-i\omega_2 t}\}, \tag{1}$$

where vector amplitudes $\mathbf{E}^{(1)}$ and $\mathbf{E}^{(2)}$ are determined by a superposition of running waves

$$\mathbf{E}^{(n)}(\mathbf{r}) = \sum_m \mathbf{E}_m^{(n)} e^{i\mathbf{k}_m^{(n)}\cdot\mathbf{r}}, \quad n = 1, 2. \tag{2}$$

The directions of the waves' propagation are given by wave vectors $\mathbf{k}_m^{(n)}$. The frequencies of the light-field components ω_1 and ω_2 are near the resonance lines D_2 and D_1 of lithium atoms, respectively. The scheme of energy levels and optical transitions used for laser cooling of ^{6}Li atoms is shown in Fig. 1.

It should be noted that the hyperfine splitting of the $^2P_{3/2}$ and $^2P_{1/2}$ states for lithium atoms is comparable to the natural linewidth $\gamma/2\pi = 5.9$ MHz. Moreover, the hyperfine components of the $^2P_{3/2}$ state are within the natural linewidth γ, which requires the use of a model taking into account the interaction of light waves with all hyperfine components. Further, to simplify notation, we introduce the indices e_α ($\alpha = 1, \ldots, 5$) for the hyperfine components of the excited states $^2P_{3/2}$ and $^2P_{1/2}$, and g_n ($n = 1, 2$) for the hyperfine components of the ground state $^2S_{1/2}$ (see Fig. 1). Note that ^{7}Li and ^{6}Li isotopes have a similar level structure. Here we perform our analysis for the ^{6}Li atoms that have lower values of total angular momentum. However, the results can also be generalized for ^{7}Li atoms as well.

The kinetics of atoms in light fields is described by the quantum kinetic equation for the atomic density matrix

$$\frac{\partial}{\partial t}\hat{\rho} = -\frac{i}{\hbar}[\hat{H}_{\mathrm{kin}} + \hat{H}_{\mathrm{int}} + \widehat{W}(t), \hat{\rho}] + \hat{\Gamma}\{\hat{\rho}\}, \tag{3}$$

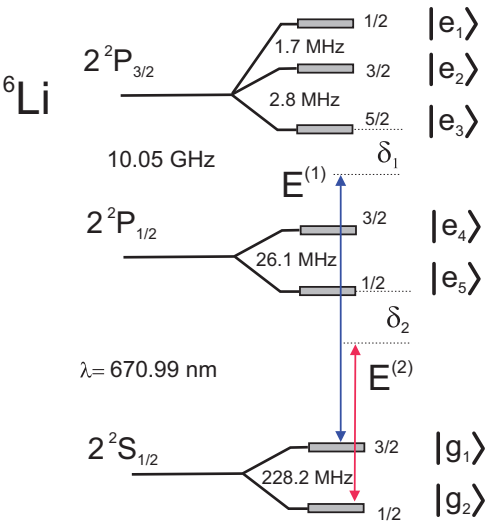

FIG. 1. Level structure of ^{6}Li atom.

where $\hat{H}_{\mathrm{kin}} = \hat{p}^2/2M$ is the kinetic part, $\widehat{W}(t) = -\hat{\mathbf{d}}\cdot\mathbf{E}(\mathbf{t})$ describes the interaction with the field in the dipole approximation (where $\hat{\mathbf{d}}$ is the dipole moment operator), and $\hat{H}_{\mathrm{int}}$ is the Hamiltonian of a free atom in the rest frame

$$\hat{H}_{\mathrm{int}} = \sum_{\alpha=1,\ldots,5} \mathcal{E}_{e_\alpha}\hat{P}^{(e_\alpha)} + \sum_{n=1,2} \mathcal{E}_{g_n}\hat{P}^{(g_n)}, \tag{4}$$

where $\mathcal{E}_{e_\alpha}$ and $\mathcal{E}_{g_n}$ are energies of the excited states $|e_\alpha\rangle$ and ground states $|g_n\rangle$. Here $\hat{P}^{(e_\alpha)}$ and $\hat{P}^{(g_n)}$ are projection operators onto the Zeeman components of the hyperfine level $|e_\alpha\rangle$ and $|g_n\rangle$,

$$\hat{P}^{(e_\alpha)} = \sum_{\mu_{e_\alpha}=-F_{e_\alpha}}^{F_{e_\alpha}} |F_{e_\alpha}, \mu_{e_\alpha}\rangle\langle F_{e_\alpha}, \mu_{e_\alpha}|, \quad \alpha = 1, \ldots, 5$$

$$\hat{P}^{(g_n)} = \sum_{\mu_{g_n}=-F_{g_n}}^{F_{g_n}} |F_{g_n}, \mu_{g_n}\rangle\langle F_{g_n}, \mu_{g_n}|, \quad n = 1, 2. \tag{5}$$

The operator $\hat{\Gamma}\{\hat{\rho}\}$ describes the relaxation of an atom due to spontaneous emission.

To use the resonant approximation in a bichromatic field (1), let us introduce the operator

$$\hat{T} = \exp\left[-it\left(\sum_{\alpha=1,2,3}\omega_1\hat{P}^{(e_\alpha)} + \sum_{\alpha=4,5}\omega_2\hat{P}^{(e_\alpha)}\right)\right], \tag{6}$$

where the summation is taken over all components of the levels $^2P_{3/2}$ and $^2P_{1/2}$. For the transformation (6), the evolution equation for the transformed density matrix $\hat{\tilde{\rho}} = \hat{T}^\dagger\hat{\rho}\,\hat{T}$ takes a similar form to (3)

$$\frac{\partial}{\partial t}\hat{\tilde{\rho}} = -\frac{i}{\hbar}[\hat{H}_{\mathrm{kin}} + \widehat{\widetilde{H}}_{\mathrm{int}} + \widehat{\widetilde{W}}, \hat{\tilde{\rho}}] + \hat{\Gamma}\{\hat{\tilde{\rho}}\}. \tag{7}$$

However, the resonance approximation allows to eliminate the time dependence in the interaction operator and divide it into the sum of contributions

$$\widehat{\widetilde{W}} = \hbar\hat{V}^{(1)} + \hbar\hat{V}^{(2)} + \mathrm{H.c.}, \tag{8}$$

determined by the interaction with two frequency components: $\mathbf{E}^{(1)}$ is close to the resonance with D_2 line and $\mathbf{E}^{(2)}$ is close to the resonance with D_1 line (Fig. 1)

$$\hat{V}^{(1)} = \hat{V}^{e_1 g_1} + \hat{V}^{e_2 g_1} + \hat{V}^{e_3 g_1}, \hat{V}^{(2)} = \hat{V}^{e_4 g_2} + \hat{V}^{e_5 g_2}. \quad (9)$$

Here, the operator blocks $\hat{V}^{e_\alpha g_n}$ are defined as

$$\hat{V}^{e_\alpha g_n} = -(\mathbf{E}^{(n)} \cdot \hat{\mathbf{D}}^{e_\alpha g_n})\bar{d}/\hbar, \quad (10)$$

where $\bar{d}$ is the reduced matrix element of the dipole moment operator and $\hat{\mathbf{D}}^{e_\alpha g_n}$ are the matrix blocks of dipole moment operator

$$\hat{\mathbf{d}} = \hat{\mathbf{D}}\,\bar{d} + \text{ H.c.}. \quad (11)$$

Thus the the matrix blocks $\hat{\mathbf{D}}^{e_\alpha g_n}$ are

$$\hat{\mathbf{D}}^{e_\alpha g_n} = \hat{P}^{(e_\alpha)}\,\hat{\mathbf{D}}\,\hat{P}^{(g_n)}. \quad (12)$$

The decomposition of the dipole moment operator $\hat{\mathbf{D}}$ in circular basis

$$\hat{\mathbf{D}} = \sum_{q=0,\pm1} \hat{D}_q\,\mathbf{e}^q, \quad (13)$$

is determined by the corresponding matrix elements $\langle I, J_{e_\alpha}; F_{e_\alpha}, \mu_{e_\alpha}|\hat{D}_q|I, J_{g_n}; F_{g_n}, \mu_{g_n}\rangle$ for atomic states with electronic angular momenta of the ground and excited states: $J_{g_n} = 1/2$ and $J_{e_\alpha} = 1/2,\ 3/2$ (Fig. 1). Here I is the nuclear spin ($I = 1$ for ^{6}Li atoms). According to the Wigner-Eckart theorem [26], matrix elements are expressed through Clebsch-Gordan coefficients and 6-j symbols

$$\begin{aligned}&\langle I, J_{e_\alpha}; F_{e_\alpha}, \mu_{e_\alpha}|\hat{D}_q|I, J_{g_n}; F_{g_n}, \mu_{g_n}\rangle \\ &= C^{F_{e_\alpha},\mu_e}_{F_{g_n},\mu_{g_n};1,q}(-1)^{(J_{e_\alpha}+F_{g_n}+I+1)}\sqrt{(2F_{g_n}+1)(2J_{e_\alpha}+1)} \\ &\quad\times \begin{Bmatrix} J_{e_\alpha} & 1 & F_{g_n} \\ J_{g_n} & I & J_{e_\alpha}\end{Bmatrix}. \end{aligned} \quad (14)$$

The non-Hamiltonian evolution of the system due to spontaneous emission of the light-field photons is described by $\hat{\Gamma}\{\hat{\tilde{\rho}}\}$ in the equation for the density matrix (3) and (7). Taking into account the recoil effects, this contribution has the form (see, for example, [15,16])

$$\hat{\Gamma}\{\hat{\tilde{\rho}}\} = -\frac{\gamma}{2}(\hat{P}^{(e)}\hat{\tilde{\rho}} + \hat{\tilde{\rho}}\,\hat{P}^{(e)}) + \hat{\gamma}\{\hat{\tilde{\rho}}\}, \quad (15)$$

with

$$\begin{aligned}&\hat{\gamma}\{\hat{\tilde{\rho}}\} \\ &= \gamma\frac{3}{2}\left\langle \sum_{\xi=1,2}(\hat{\mathbf{D}}\cdot\mathbf{e}_\xi(\mathbf{k}_\xi))^\dagger e^{-i\mathbf{k}_\xi\cdot\hat{\mathbf{r}}}\hat{\tilde{\rho}}\,e^{i\mathbf{k}_\xi\cdot\hat{\mathbf{r}}}(\hat{\mathbf{D}}\cdot\mathbf{e}_\xi(\mathbf{k}_\xi))\right\rangle_{\Omega_\xi}. \end{aligned} \quad (16)$$

Here the operator $\hat{P}^{(e)} = \sum_\alpha \hat{P}^{(e_\alpha)}$ is a projector onto excited states (the summation is taken over all states of the $^2P_{3/2}$ and $^2P_{1/2}$ levels), $\langle\ldots\rangle_{\Omega_\xi}$ means averaging over the angles of spontaneously emitted photons with two orthogonal polarizations $\mathbf{e}_\xi$, ($\xi = 1, 2$), the wave vectors $\mathbf{k}_\xi$ are specifying the direction of spontaneously emitted photon, and $\hat{\mathbf{r}}$ is the position operator.

The Hamiltonian of a free atom in the rest frame in the rotating basis (6) takes the form

$$\hat{\widetilde{H}}_{\text{int}} = -\hbar\sum_{\alpha=1..5}\Delta_\alpha\,\hat{P}^{(e_\alpha)}, \quad (17)$$

where

$$\begin{aligned}\Delta_\alpha &= \omega_1 - \omega_{e_\alpha g_1},\ \text{for } \alpha = 1, 2, 3, \\ \Delta_\alpha &= \omega_2 - \omega_{e_\alpha g_2},\ \text{for } \alpha = 4, 5, \end{aligned} \quad (18)$$

are detunings from resonance for light-induced transitions between hyperfine levels of D_2 and D_1 lines caused by two frequency components Fig. 1. Here $\omega_{e_\alpha g_n} = (\mathcal{E}_{e_\alpha} - \mathcal{E}_{g_n})/\hbar$ is the transition frequency between states $|e_\alpha\rangle$ and $|g_n\rangle$.

Note that the kinetics of lithium atoms is characterized by enough of a small recoil parameter $\varepsilon_R = E_R/\hbar\gamma \simeq 0.01$ ($E_R = \hbar^2k^2/2M$ is the recoil energy) that makes it possible to use the semiclassical approximation. Indeed, for such a small recoil parameter, the semiclassical approximation gives a good agreement with quantum treatment based on the direct numerical solution of the density matrix equation (7) in monochromatic light [27,28]. Within the semiclassical approximation, the equation for the density matrix (7) can be reduced to the Fokker-Planck equation (see, for example, [29–31])

$$\begin{aligned}\left(\frac{\partial}{\partial t} + \frac{\mathbf{p}}{M}\cdot\nabla\right)\mathcal{F} &= -\sum_i \frac{\partial}{\partial p_i}f_i(\mathbf{r},\mathbf{p})\mathcal{F} \\ &\quad + \sum_{i,j}\frac{\partial^2}{\partial p_i\,\partial p_j}D_{ij}(\mathbf{r},\mathbf{p})\mathcal{F}, \end{aligned} \quad (19)$$

for the distribution function of atoms in the phase space $\mathcal{F}(\mathbf{r},\mathbf{p}) = \text{Tr}\{\hat{\rho}(\mathbf{r},\mathbf{p})\}$, where the trace is taken over the internal degrees of the atom density matrix in the Wigner representation. Here ∇ is the spatial gradient, f_i are the Cartesian components of the light force on atoms, and D_{ij} are the Cartesian components of the diffusion tensor in momentum space. The force and diffusion tensor can be obtained in a process of reduction of the density matrix equation (3) to the Fokker-Plank equation (19).

III. BICHROMATIC OPTICAL LATTICE FOR LITHIUM ATOMS

The light force on atom in a light field is determined by the spatial gradients of the interaction operator (8)

$$f_i(\mathbf{r},\mathbf{v}) = -\text{Tr}\{(\nabla_i\,\hat{\widetilde{W}}(\mathbf{r}))\,\hat{\sigma}(\mathbf{r},\mathbf{v})\}, \quad (20)$$

where $\hat{\sigma}(\mathbf{r},\mathbf{v})$ is the stationary solution of equation (7) in zero order by the recoil effects

$$(\mathbf{v}\cdot\nabla)\,\hat{\sigma}(\mathbf{r},\mathbf{v}) = -\frac{i}{\hbar}[\hat{\widetilde{H}}_{\text{int}} + \hat{\widetilde{W}}(\mathbf{r}),\hat{\sigma}(\mathbf{r},\mathbf{v})] + \hat{\Gamma}^{(0)}\{\hat{\sigma}(\mathbf{r},\mathbf{v})\}, \quad (21)$$

with the normalization condition $\text{Tr}\{\hat{\sigma}\} = 1$. The operator of spontaneous relaxation in zeroth order by recoil

is

$$\hat{\Gamma}^{(0)}\{\hat{\sigma}\} = -\frac{\gamma}{2}(\hat{P}^{(e)}\hat{\sigma} + \hat{\sigma}\,\hat{P}^{(e)}) + \hat{\gamma}^{(0)}\{\hat{\sigma}\},$$
$$\hat{\gamma}^{(0)}\{\hat{\sigma}\} = \gamma \sum_{q=0,\pm1} \hat{D}_q^{\dagger}\,\hat{\sigma}\,\hat{D}_q. \tag{22}$$

Let us note, that expression (20) defines the general expression for the force as a function of atom position $\mathbf{r}$ and velocity $\mathbf{v}$. The optical lattice, the optical potential for atoms is determined by the force on moveless atom $v = 0$. The expression for the force can be obtained numerically based on the solution of (21) for the density matrix $\hat{\sigma}$, however, analytical solutions are of the greatest interest for analysis.

The force, by its nature, is divided into two components: the induced force, associated with the transmission of momentum from the light field to an atom in the processes of stimulated absorption or emission of photons between different spatial modes of the field, and the spontaneous light pressure force, associated with the transfer of momentum to atoms in the cycle of induced absorption and the spontaneous emission of photons. Both components of the force can lead to the formation of an optical potential, or the so-called optical lattice [2,8,9,32].

For analysis of the optical potential in a bichromatic field, we can get the analytical expression for the force on slow atoms $kv < \gamma$ in the light fields of low intensity

$$S^{(n)} = \frac{|\Omega^{(n)}(\mathbf{r})|^2}{\gamma^2 + 4\delta_n^2} \ll 1, \quad n = 1, 2, \tag{23}$$

where

$$\Omega^{(n)}(\mathbf{r}) = -\frac{|\mathbf{E}^{(n)}(\mathbf{r})|\bar{d}}{\hbar}, \tag{24}$$

is the local Rabi frequency for nth frequency component (2)

$$\delta_1 = \omega_1 - \omega_{e_3g_1}, \quad \delta_2 = \omega_2 - \omega_{e_5g_2}, \tag{25}$$

are the main detunings from the resonances, which are determined by the frequency $\omega_{e_3g_1}$ of the transition $^2P_{3/2}(F = 5/2) \to {}^2S_{1/2}(F = 3/2)$ for component $\mathbf{E}^{(1)}$ and the frequency $\omega_{e_5g_2}$ of the transition $^2P_{1/2}(F = 1/2) \to {}^2S_{1/2}(F = 1/2)$ for component $\mathbf{E}^{(2)}$ as shown in Fig. 1.

In the limit (23), the populations of the excited states are small, and for slow atoms $kv < \gamma$ equation (21) can be reduced to the equation for the density matrices of two ground states $^2S_{1/2}$ with angular momenta $F = 3/2$ and $F = 1/2$,

$$\hat{\sigma}^{(n)} = \hat{P}^{(g_n)}\hat{\sigma}\,\hat{P}^{(g_n)}, \quad n = 1, 2. \tag{26}$$

In this case, the equations for these matrices take the form

$$(\mathbf{v}\cdot\boldsymbol{\nabla})\hat{\sigma}^{(1)} = -i\big[\hat{H}_{\rm eff}^{(1)}, \hat{\sigma}^{(1)}\big] + \hat{P}^{(g_1)}\,\hat{\gamma}^{(0)}\{\hat{\sigma}^{ee}\}\,\hat{P}^{(g_1)},$$
$$(\mathbf{v}\cdot\boldsymbol{\nabla})\hat{\sigma}^{(2)} = -i\big[\hat{H}_{\rm eff}^{(2)}, \hat{\sigma}^{(2)}\big] + \hat{P}^{(g_2)}\,\hat{\gamma}^{(0)}\{\hat{\sigma}^{ee}\}\,\hat{P}^{(g_2)}. \tag{27}$$

The Hamiltonian evolution here is described by two effective Hamiltonians

$$\hat{H}_{\rm eff}^{(1)} = \sum_{\alpha=1,2,3} \frac{\Delta_\alpha - i\gamma/2}{|\nu_\alpha|^2}\,(\hat{V}^{e_\alpha g_1})^{\dagger}\hat{V}^{e_\alpha g_1},$$
$$\hat{H}_{\rm eff}^{(2)} = \sum_{\alpha=4,5} \frac{\Delta_\alpha - i\gamma/2}{|\nu_\alpha|^2}\,(\hat{V}^{e_\alpha g_2})^{\dagger}\hat{V}^{e_\alpha g_2}. \tag{28}$$

Here we use the notation $\nu_\alpha = \gamma/2 - i\,\Delta_\alpha$. The density matrix of the excited states $\hat{\sigma}^{ee}$ in the zeroth order by recoil for slow atoms is divided into a sum of two blocks

$$\hat{\sigma}^{ee} = \hat{\sigma}_1^{ee} + \hat{\sigma}_2^{ee},$$
$$\hat{\sigma}_1^{ee} = \sum_{\alpha,\alpha'=1,2,3} \frac{1}{\nu_\alpha\,\nu_{\alpha'}^*}\,\hat{V}^{e_\alpha g_1}\,\hat{\sigma}^{(1)}\,(\hat{V}^{e_{\alpha'} g_1})^{\dagger},$$
$$\hat{\sigma}_2^{ee} = \sum_{\alpha,\alpha'=4,5} \frac{1}{\nu_\alpha\,\nu_{\alpha'}^*}\,\hat{V}^{e_\alpha g_2}\,\hat{\sigma}^{(2)}(\hat{V}^{e_{\alpha'} g_2})^{\dagger}. \tag{29}$$

Note, that for sufficiently large detunings that exceed the hyperfine splitting in excited states $^2P_{3/2}$ and $^2P_{1/2}$ and the natural width γ, i.e.,

$$\delta_1 \gg (\omega_{e_1e_2},\ \omega_{e_2e_3},\ \gamma),\ \delta_2 \gg (\omega_{e_4e_5},\ \gamma), \tag{30}$$

the following approximation can be used

$$\Delta_\alpha \simeq \delta_1 \ \text{ for } \alpha = 1, 2, 3,\ \Delta_\alpha \simeq \delta_2 \ \text{ for } \alpha = 4, 5. \tag{31}$$

In this case, the effective Hamiltonians (28) are substantially simplified and reduced to the shift operators for the hyperfine components of the ground states

$$\hat{H}_{eff}^{(n)}(\mathbf{r}) = \delta_n\,S^{(n)}(\mathbf{r})\,\hat{U}^{(n)}(\mathbf{r}), \quad n = 1, 2,$$
$$\hat{U}^{(1)}(\mathbf{r}) = \frac{2}{3}|\mathbf{A}_1(\mathbf{r})|^2\,\hat{P}^{(g_1)} - \frac{i}{3}\left([\mathbf{A}_1^*(\mathbf{r})\times\mathbf{A}_1(\mathbf{r})]\cdot\frac{\hat{\mathbf{F}}}{F_{g_1}}\right),$$
$$\hat{U}^{(2)}(\mathbf{r}) = \frac{1}{3}|\mathbf{A}_2(\mathbf{r})|^2\,\hat{P}^{(g_2)} - \frac{i}{9}\left([\mathbf{A}_2^*(\mathbf{r})\times\mathbf{A}_2(\mathbf{r})]\cdot\frac{\hat{\mathbf{F}}}{F_{g_2}}\right), \tag{32}$$

are determined by the spatial configuration of local polarization vectors for each frequency component $\mathbf{A}_1(\mathbf{r}) = \mathbf{E}^{(1)}(\mathbf{r})/|\mathbf{E}^{(1)}(\mathbf{r})|$ and $\mathbf{A}_2(\mathbf{r}) = \mathbf{E}^{(2)}(\mathbf{r})/|\mathbf{E}^{(2)}(\mathbf{r})|$. Here $\hat{\mathbf{F}}$ is the total angular momentum operator and $[\mathbf{A}\times\mathbf{B}]$ denotes the cross product of the vectors $\mathbf{A}$ and $\mathbf{B}$. Expressions (32) are written in the invariant form and valid for an arbitrary nuclear spin (i.e., they are also applicable to ^{7}Li atoms). Note that the expression for $\hat{U}^{(1)}$ corresponds to the optical lattice light shift in [33,34] obtained for the monochromatic light field far detuned to the optical resonance D_2 line of Cs atoms.

In the considered limit (23), the force on atoms can be represented as a sum of two parts

$$\mathbf{f} = \hbar\,\mathrm{Tr}\{\hat{\mathbf{f}}_1\,\hat{\sigma}^{(1)}\} + \hbar\,\mathrm{Tr}\{\hat{\mathbf{f}}_2\,\hat{\sigma}^{(2)}\}, \tag{33}$$

where the force vector operators $\hat{\mathbf{f}}_n$ are determined by the spatial gradients

$$\hat{\mathbf{f}}_n = -\boldsymbol{\nabla}\hat{H}_{\rm eff}^{(n)}, \quad n = 1, 2. \tag{34}$$

It should be noted that a distinctive feature of the considered bichromatic configuration, compared to optical lattices formed by monochromatic fields, is the presence of an additional shift $\hat{U}^{(2)}$ with a spatial dependence that may be different from $\hat{U}^{(1)}$. Spatially nonuniform optical pumping of the ground state levels $|g_1\rangle$ and $|g_2\rangle$, defined by equation (27) under the motion in two potentials, leads to the rectification of the dipole force (33) on the wavelength scale. As a result, the optical potential with a macroscopic period can be formed. To demonstrate this, we consider several examples below.

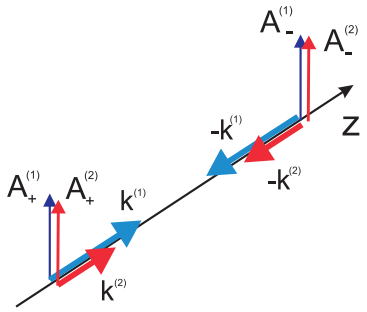

FIG. 2. Double lin||lin field configuration.

A. One-dimensional optical lattices created by a bichromatic field

Let us consider the general form of a one-dimensional bichromatic field configuration created by counterpropagating waves of equal scalar amplitude along the z axis

$$\mathbf{E}^{(n)}(z) = E_0^{(n)}(\mathbf{A}_+^{(n)} e^{ik^{(n)}z} + \mathbf{A}_-^{(n)} e^{-ik^{(n)}z}), \quad n = 1, 2. \tag{35}$$

Here $E_0^{(n)}$ are scalar amplitudes and $\mathbf{A}_\pm^{(n)}$ are unit polarization vectors of the counterpropagating light waves of different frequency components ($n = 1, 2$), which can be elliptical in the general case. If we denote $k^{(2)} = k$ and $\Delta k = k^{(1)} - k^{(2)} > 0$, then the field (35) can be rewritten as

$$\begin{aligned}\mathbf{E}^{(1)}(z) &= E_0^{(1)}(\mathbf{A}_+^{(1)} e^{ikz+i\Delta\phi} + \mathbf{A}_-^{(1)} e^{-ikz-i\Delta\phi}),\\ \mathbf{E}^{(2)}(z) &= E_0^{(2)}(\mathbf{A}_+^{(2)} e^{ikz} + \mathbf{A}_-^{(2)} e^{-ikz}).\end{aligned} \tag{36}$$

Since $\Delta k = k^{(1)} - k^{(2)} \ll k$, the relative spatial phase

$$\Delta\phi = \Delta k\, z, \tag{37}$$

can be considered constant over the wavelength scale $\lambda = 2\pi/k$. The spatial polarization configurations of different frequency components are determined by the mutual spatial orientation of the polarization vectors $\mathbf{A}_+^{(n)}$ and $\mathbf{A}_-^{(n)}$. Below we consider several configurations.

1. *Double* lin||lin *field configuration*

For a bichromatic field created by standing waves with identical linear polarizations $\mathbf{A}_\pm^{(1)} = \mathbf{A}_\pm^{(2)} = \mathbf{A} = \mathbf{A}^*$ (the so-called double lin||lin configuration, see Fig. 2), the effective Hamiltonians (32) in the limit of large detunings (30) are reduced to the scalar light shifts $u_1 = 2\delta_1 S_1 |\mathbf{A}|^2/3$ and $u_2 = \delta_2 S_2 |\mathbf{A}|^2/3$ with a spatial dependence represented by standing waves of each frequency component

$$\begin{aligned}\hat{H}_{\text{eff}}^{(n)} &= u_n \hat{P}^{(g_n)}, \text{ for } n = 1, 2,\\ u_1 &= \frac{8}{3}\delta_1 s_1 \cos^2(kz + \Delta\phi),\\ u_2 &= \frac{4}{3}\delta_2 s_2 \cos^2(kz).\end{aligned} \tag{38}$$

Here s_1 and s_2 are the saturation parameters per one running wave, $s_n = |\Omega_0^{(n)}|^2/(4\delta_n^2 + \gamma^2)$, where $\Omega_0^{(n)} = -E_0^{(n)}\bar{d}/\hbar$ are the corresponding Rabi frequencies. The optical potential of the light field is determined by the force (20) and (33) on the atom at rest. The solution of (27) for $v = 0$ in this field leads to an isotropic distribution on each of the ground levels $|g_1\rangle$ and $|g_2\rangle$

$$\begin{aligned}\hat{\sigma}^{(1)} &= \frac{\cos^2(kz)\, s_2}{2s_1\cos^2(kz + \Delta\phi) + 4s_2\cos^2(kz)}\hat{P}^{(g_1)},\\ \hat{\sigma}^{(2)} &= \frac{\cos^2(kz + \Delta\phi)\, s_1}{2s_1\cos^2(kz + \Delta\phi) + 4s_2\cos^2(kz)}\hat{P}^{(g_2)},\end{aligned} \tag{39}$$

since $[\mathbf{A}_n^* \times \mathbf{A}_n] = 0$ in (32) for this field configuration Fig. 2. Thus, the force (33) resulting in the formation of an optical potential is divided into two contributions from each of the frequency components

$$\begin{aligned}f &= f_1 + f_2,\\ f_1 &= \hbar k\frac{16}{3}\frac{\delta_1 s_1 s_2 \sin(2kz + 2\Delta\phi)\cos^2(kz)}{s_1\cos^2(kz + \Delta\phi) + 2s_2\cos^2(kz)},\\ f_2 &= \hbar k\frac{4}{3}\frac{\delta_2 s_1 s_2 \sin(2kz)\cos^2(kz + \Delta\phi)}{s_1\cos^2(kz + \Delta\phi) + 2s_2\cos^2(kz)}.\end{aligned} \tag{40}$$

As was mentioned above, due to the different spatial dependencies of the light shifts u_1, u_2 and the spatially inhomogeneous optical pumping of $|g_1\rangle$ and $|g_2\rangle$ states, the effect of force rectification on the wavelength scales appears. This rectification effect is similar in nature to those described for a two-level atom in a bichromatic field [18,20,24,25], as well as in monochromatic fields formed by counterpropagating waves with elliptical polarizations [35]. Thus, the average over the wavelength force

$$\bar{f}(\Delta\phi) = \frac{1}{\lambda}\int_0^\lambda f(z)\, dz = \bar{f}_1(\Delta\phi) + \bar{f}_2(\Delta\phi), \tag{41}$$

in the general case is not equal to zero, and its magnitude and sign are determined by the relative spatial phase $\Delta\phi$

$$\begin{aligned}\bar{f}_1 &= \hbar k\frac{16}{3}\frac{\delta_1 s_1 s_2 \sin(2\Delta\phi)}{[8s_1 s_2\cos^2(\Delta\phi) + (2s_2 - s_1)^2]^2}\Big\{|\sin(\Delta\phi)|\sqrt{2s_1 s_2}[(2s_2 + 3s_1)(2s_2 - s_1) - 8s_2 s_1\cos^2(\Delta\phi)]\\ &\quad + 16s_2^2 s_1\cos^2(\Delta\phi) - s_1(6s_2 + s_1)(2s_2 - s_1)\Big\},\\ \bar{f}_2 &= \hbar k\frac{4}{3}\frac{\delta_2 s_1 s_2 \sin(2\Delta\phi)}{[8s_1 s_2\cos^2(\Delta\phi) + (2s_2 - s_1)^2]^2}\Big\{|\sin(\Delta\phi)|\sqrt{2s_1 s_2}[(6s_2 + s_1)(2s_2 - s_1) + 8s_2 s_1\cos^2(\Delta\phi)]\\ &\quad - 8s_2 s_1^2\cos^2(\Delta\phi) - 2s_2(2s_2 + 3s_1)(2s_2 - s_1)\Big\}.\end{aligned} \tag{42}$$

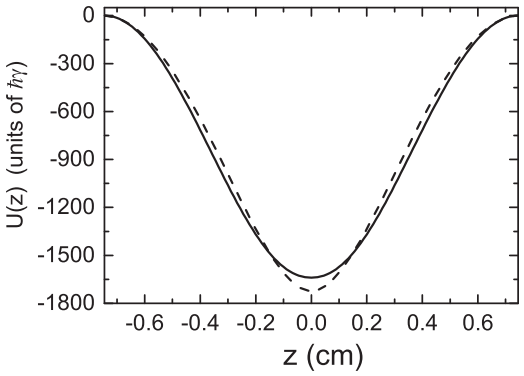

FIG. 3. Macroscopic optical potential $U(z)$ in units of $\hbar\gamma$ of a bichromatic lattice formed by the field of double lin||lin configuration. The solid line represents the solution based on the analytical expressions obtained in the approximation of small saturation and large detunings (40), while the dotted line represents the optical lattice potential obtained by direct numerical solution for the force (20), i.e., outside the indicated approximations. The detunings are $\delta_1 = -2\gamma$ and $\delta_2 = -3\gamma$, the saturation parameters are $s_1 = s_2 = 0.1$ (i.e., Rabi per one wave $\Omega_0^{(1)} \simeq 1.3\gamma$, $\Omega_0^{(2)} \simeq 1.9\gamma$). The depth of macroscopic optical potential for considered parameters reaches $\Delta U = 1720\,\hbar\gamma$ that corresponds $\simeq 0.5$ K in temperature units.

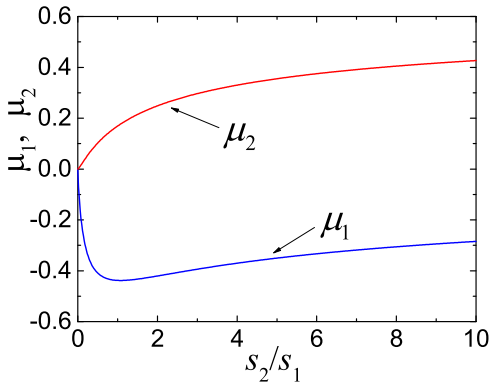

FIG. 4. The functions $\mu_1(s_2/s_1)$ and $\mu_2(s_2/s_1)$, which determine the depth of macroscopic potentials U_1 and U_2 in the field of double lin||lin configuration.

As the result, on a distance exceeding the wavelength, the rectified force components $\bar{f}_1$ and $\bar{f}_2$ form a deep macroscopic potential

$$U(z) = -\int \bar{f}_1(\Delta\phi(z))\,dz - \int \bar{f}_2(\Delta\phi(z))\,dz = U_1(z) + U_2(z), \tag{43}$$

with a period corresponding to the change of the relative spatial phase $\Delta\phi$ from 0 to π, which, for the lithium atoms in the one-dimensional field (35) is $\Lambda \simeq 1.5$ cm (see Fig. 3). In this case, the positions of the global maxima and minima of the potentials U_n (43) correspond to position where $\Delta\phi = 0, \pm\pi/2, \ldots$. The depth of each term in (43) is determined by

$$\Delta U_n = \frac{1}{\Delta k}\int_0^{\pi/2} \bar{f}_n(\Delta\phi)\,d\Delta\phi, \quad n = 1, 2, \tag{44}$$

which results the following expressions for potentials depth:

$$\Delta U_1 = \hbar\delta_1 \frac{k}{\Delta k} s_1 \mu_1(s_2/s1),$$
$$\Delta U_2 = \hbar\delta_2 \frac{k}{\Delta k} s_1 \mu_2(s_2/s1). \tag{45}$$

The μ_1 and μ_2 here are dimensionless functions of the ratio $a = s_2/s_1$ (see Fig. 4)

$$\mu_1(a) = -\frac{8}{3}\,a\left[\ln\left(\frac{2a+1}{(\sqrt{2a}+1)^2}\right) + \frac{2}{\sqrt{2a}+1}\right],$$
$$\mu_2(a) = \frac{1}{3}\left[\ln\left(\frac{2a+1}{(\sqrt{2a}+1)^2}\right) + \frac{\sqrt{8a}}{\sqrt{2a}+1}\right], \tag{46}$$

which allow to estimate the depth of the macroscopic potential (43) for various light-field parameters.

The relatively large depth of the macroscopic potential, which significantly exceeds the magnitude of the light shifts of each frequency component, is provided by the multiplier $k/\Delta k$ (for lithium atoms $k/\Delta k \simeq 4.4 \times 10^4$). As the result, for parameters of Fig. 3, the depth of the macroscopic potential reaches $\simeq 0.5$ K in temperature units. However, for the localization of trapped atoms, the curvature at the points of the minimum macroscopic potential plays a significant role. In the case of bichromatic field it is proportional to $\Delta k/k$, which allows to localize the trapped Li atoms at submillimeter scales (see below).

For the bichromatic field with detunings δ_1, δ_2 near the resonant lines D_2 and D_1, the presence of the dissipative Doppler force potentially allows trapping and cooling of atoms directly from the room temperature vapor. The Doppler mechanisms of laser cooling are the result of the imbalance of spontaneous light pressure forces from counterpropagating waves on moving atoms [2] and acts on atoms over the all points of the macroscopic potential. Figure 5 shows the dependence of the force on lithium atoms as a function of atomic velocity. In particular, the force $f(v)$ for considered detunings $\delta_1 = -2\gamma$ and $\delta_2 = -3\gamma$ takes on maximum values for the velocity groups of atoms near resonance lines, near $|v| \simeq 3\gamma/k$. As can be seen here the force has a sufficiently wide velocity range, comparable to the dissipative force in a standard MOT. The result for the force here is obtained on the basis of (20), i.e.,

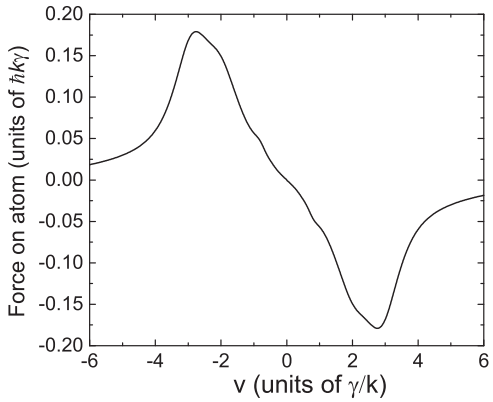

FIG. 5. The force on lithium atoms in bichromatic field as function of velocity in the region of the global minimum of the optical potential. The field parameters correspond to Fig. 3.

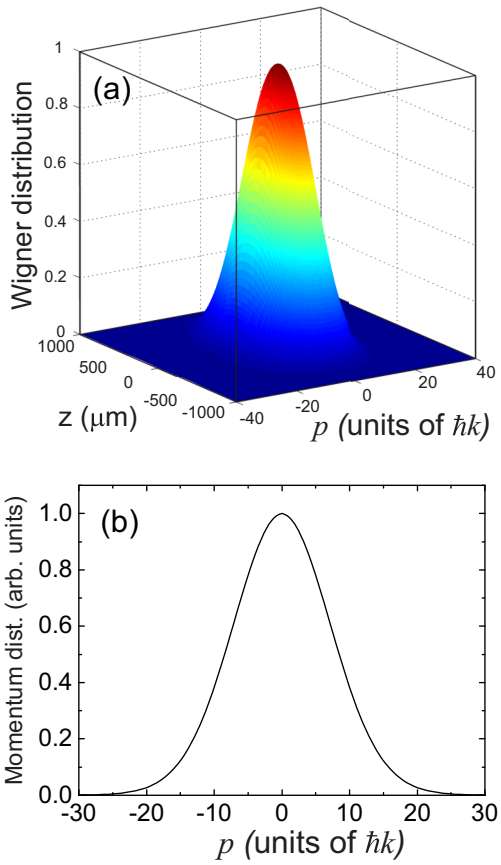

FIG. 6. The Wigner function of (a) the atomic phase distribution $\mathcal{F}(z, p)$ and (b) the momentum distribution of cold atoms in the macroscopic potential of the bichromatic field of double lin||lin configuration. The field parameters correspond to Fig. 3.

beyond the limit of the low field intensity (23) and slow atoms $kv < \gamma$.

Figure 6 shows steady-state Wigner function $\mathcal{F}(z, p)$ and the momentum distribution of atoms in the trap, obtained by solving the Fokker-Planck equation (19) by taking into account the nonlinear dependence of the force (see Fig. 5) and diffusion coefficients on the atom's velocity. For the considered parameters, the momentum distribution of atoms is well approximated by a Gaussian distribution with temperature $T \simeq 1.1\,\hbar\gamma/k_B \simeq 300\,\mu$K and corresponds to temperatures near the Doppler limit of laser cooling. The size of the cold atom cloud in a macroscopic potential can be defined as

$$\beta_z = \sqrt{\int z^2 \mathcal{F}(z, p)\, dz dp}, \tag{47}$$

where the integration by coordinate is taken over the macroscopic period. For the parameters of Fig. 6 the size of the atomic cloud is $\beta_z \simeq 320\,\mu$m.

2. *Double* lin ⊥ lin *field configuration*

To achieve laser cooling below the Doppler limit, the light fields with polarization gradients are required. In our case, such a field can be formed with counterpropagating waves with different polarizations [31,35,36]. For example, the well-known lin ⊥ lin field configuration, formed by waves with orthogonal linear polarizations, and $\sigma_+ - \sigma_-$ configuration, formed by waves with opposite circular polarizations [10]. However, the $\sigma_+ - \sigma_-$ field does not lead to spatial modulation of light shifts according to (32) in the limit of large detunings (30), and the rectification effect is absent.

In this section, we consider the double lin ⊥ lin configuration (see Fig. 7), where $\mathbf{A}_+^{(1)} = \mathbf{A}_+^{(2)} = \mathbf{e}_x$ is the unit vector along the x axis, and $\mathbf{A}_-^{(1)} = \mathbf{A}_-^{(2)} = \mathbf{e}_y$ is the unit vector along the y axis

$$\mathbf{E}^{(n)}(z) = E_0^{(n)}(\mathbf{e}_x e^{ik^{(n)}z} + \mathbf{e}_y e^{-ik^{(n)}z}), \qquad n = 1, 2. \tag{48}$$

For this field, as well as for the double lin||lin configuration, a deep macroscopic potential can be realized. The effective Hamiltonians (32) take the forms

$$\hat{H}_{\text{eff}}^{(1)} = 2\,\delta_1 s_1 \left(\frac{2}{3}\hat{P}^{(g_1)} - \frac{1}{3}\sin(2kz + \Delta\phi)\,\frac{\hat{F}}{F_{g_1}} \right),$$
$$\hat{H}_{\text{eff}}^{(2)} = 2\,\delta_2 s_2 \left(\frac{1}{3}\hat{P}^{(g_2)} - \frac{1}{9}\sin(2kz)\,\frac{\hat{F}}{F_{g_2}} \right). \tag{49}$$

The force on an atom in this field can also be divided into the sum of two parts

$$f_1 = -\hbar k \frac{8}{3}\frac{\delta_1 s_1 s_2}{Q}\cos(2kz + 2\Delta\phi)[\sin(2kz + 2\Delta\phi)\sin(2kz) + 5][2\sin(2kz + 2\Delta\phi) + \sin(2kz)],$$
$$f_2 = -\hbar k \frac{4}{3}\frac{\delta_2 s_1 s_2}{Q}\cos^2(2kz + 2\Delta\phi)\cos(kz)[2\sin(2kz + 2\Delta\phi) + \sin(2kz)],$$
$$Q = s_1 9\cos^2(2kz + 2\Delta\phi) + s_2[20 - \cos(4kz) - \cos(4kz + 4\Delta\phi) + 14\sin(2kz)\sin(2kz + \Delta\phi)]. \tag{50}$$

As in the case above, the rectified force in the double lin ⊥ lin field configuration creates a macroscopic potential that takes zero values at points where the relative phase of the fields is $\Delta\phi = 0, \pm\pi/2, \pm\pi, \ldots$. The macroscopic potential is determined by the average force over the wavelength (43). For the double lin ⊥ lin configuration, the analytical expression for the depths of the macroscopic potentials ΔU_n [see Eq. (44)] are quite complicated. However, they can also be represented in the form (45), where the dependencies of the dimensionless functions μ_1 and μ_2 on the saturation parameter ratio s_2/s_1 are presented in Fig. 8.

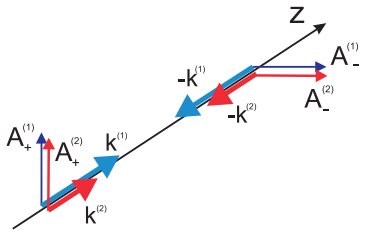

FIG. 7. Double lin ⊥ lin field configuration.

The macroscopic potential for the double field lin ⊥ lin is presented in Fig. 9. The main feature of the double lin ⊥ lin configuration is the presence of polarization gradient cooling mechanisms, which lead to the possibility of sub-Doppler cooling [10]. Indeed, for low field intensity we observe narrow distributions of trapped atoms in the phase space, as shown in Fig. 10. Note that, in the conditions of sub-Doppler cooling, the distribution of atoms in the momentum space is essentially nonequilibrium and generally cannot be described in terms of temperature. However, as shown in [37], the momentum distribution of atoms is well approximated by two-temperature Gaussian functions. The momentum distribution of trapped atoms presented in Fig. 10(b) is approximated by a two-temperature Gaussian function with temperature $T_C \simeq 0.035\,\hbar\gamma/k_B \simeq 10\,\mu$K for the "cold" fraction of atoms $N_C \simeq 20\%$, and temperature $T_H \simeq 0.5\,\hbar\gamma/k_B \simeq 140\,\mu$K for the "hot" fraction of atoms $N_H \simeq 80\%$. For the parameters of Fig. 9 the size of the trapped atom's cloud (47) in the macroscopic potential is $\beta_z \simeq 45\,\mu$m. Thus, the sub-Doppler cooling mechanisms allow to significantly decrease the trapped atom's cloud size in comparison with the double lin||lin configuration.

B. Multidimensional optical lattices created by a bichromatic field

In general, by combining bichromatic waves, as well as for monochromatic fields, one can create sufficiently complex spatial configurations of multidimensional optical lattices [8]. The spatial topology of light shifts (32) for each frequency component ω_1 and ω_2 depends not only on the chosen geometry of the waves and their polarizations, but may also depend

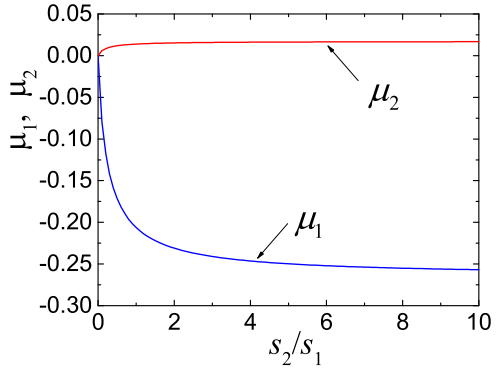

FIG. 8. The functions $\mu_1(s_2/s_1)$ and $\mu_2(s_2/s_1)$, which determine the depth of macroscopic potentials U_1 and U_2 in the field of double lin ⊥ lin configuration.

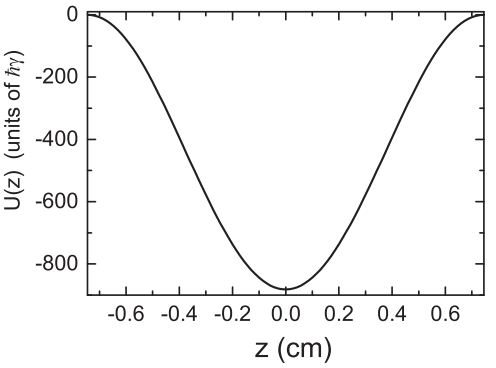

FIG. 9. Macroscopic optical potential $U(z)$ in units of $\hbar\gamma$ of a bichromatic lattice formed by the field of double lin ⊥ lin configuration. The detunings are $\delta_1 = -1.5\gamma$ and $\delta_2 = -\gamma$, the saturation parameters are $s_1 = 0.1$, $s_2 = 0.3$. The depth of the macroscopic optical potential for the considered parameters reaches $\Delta U = 890\,\hbar\gamma$ that corresponds $\simeq 0.25$ K in temperature units.

on the relative phases of the light waves forming the field of each frequency component separately. The phase dependence of the topology of optical lattices poses certain challenges for their experimental implementation and requires some efforts

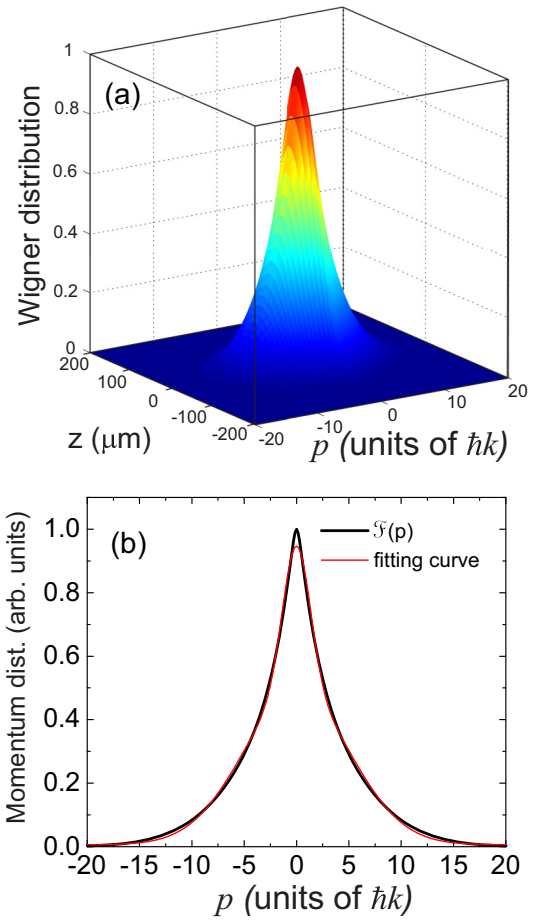

FIG. 10. The Wigner function of (a) the atomic phase distribution $\mathcal{F}(z, p)$ and (b) momentum distribution of cold atoms in the macroscopic potential of the bichromatic field of double lin ⊥ lin configuration. The waves' parameters correspond to Fig. 9.

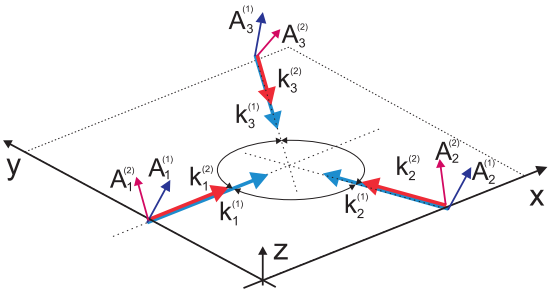

FIG. 11. Two-dimensional configuration of bichromatic optical lattice with phase-independent topology.

to control and stabilize the phase of the light waves forming the field [38]. Nevertheless, among all the diversity, it is possible to distinguish phase-independent configurations of optical lattices. Thus, in the case where the number of waves M forming the field for each of the frequency components exceeds the dimension of the space N by 1, $M = N + 1$, then the light shifts formed by each frequency component (32) have a phase-independent topology [8]. We also note that the processes of optical pumping between the ground-state levels $|g_1\rangle$ and $|g_2\rangle$ are determined by quadratic combinations of the amplitudes of the light waves of each frequency component individually (27) to (29), and are not dependent on the relative temporal phases between different frequency components of the bichromatic field. Thus, for the field configuration leading to the phase-independent topology of monochromatic lattices, the bichromatic field configuration will also lead to a phase-independent topology for a bichromatic lattice with a macroscopic period for lithium atoms.

An example of a two-dimensional (2D) configuration of fields forming a phase-independent bichromatic optical lattice is presented in Fig. 11, where the angles between the wave vectors of the running waves are 120°. Figure 12 shows the spatial dependencies of the optical potentials formed by three pairs of waves in a symmetric configuration of Fig. 11. There are two cases represented: the waves with linear polarization along the z axis [see Fig. 12(a)], and the waves with linear polarizations oriented at an angle $\varphi = \pi/4$ to the z axis [see Fig. 12(b)]. In the second case, the field, in addition to spatial nonuniform intensity, also has spatial nonuniformity of the local polarization parameters (ellipticity and orientation) of the fields $\mathbf{E}^{(1)}(\mathbf{r})$ and $\mathbf{E}^{(2)}(\mathbf{r})$. As is well known, the spatial nonuniformity of polarization leads to sub-Doppler mechanisms of laser cooling [11,12]. The periods of macroscopic potential formed by three pairs of light waves in Fig. 11 along the x and y axes are

$$\Lambda_x = \frac{\lambda}{3}\frac{k}{\Delta k} \simeq 1.9 \text{ cm}, \ \Lambda_y = \frac{\lambda}{\sqrt{3}}\frac{k}{\Delta k} \simeq 3.4 \text{ cm}. \quad (51)$$

Note that the depths of the bichromatic potentials Figs. 12(a) and 12(b) in order of magnitude correspond to the potential depths for the one-dimensional configurations in Figs. 3 and, 9 respectively.

An alternative way to avoid phase dependence in the topology of the multidimensional optical trap formed by a combination of bichromatic standing waves is to use the waves along different directions with slightly shifted frequencies. For the frequency shift of a few MHz the mutual phase gets enough fast oscillation and is much faster then the rate of the kinetic evolution processes. In this case the atom's motion will be determined by the phase-averaged dissipative force that also forms 2D or three-dimensional (3D) optical traps with macroscopic period.

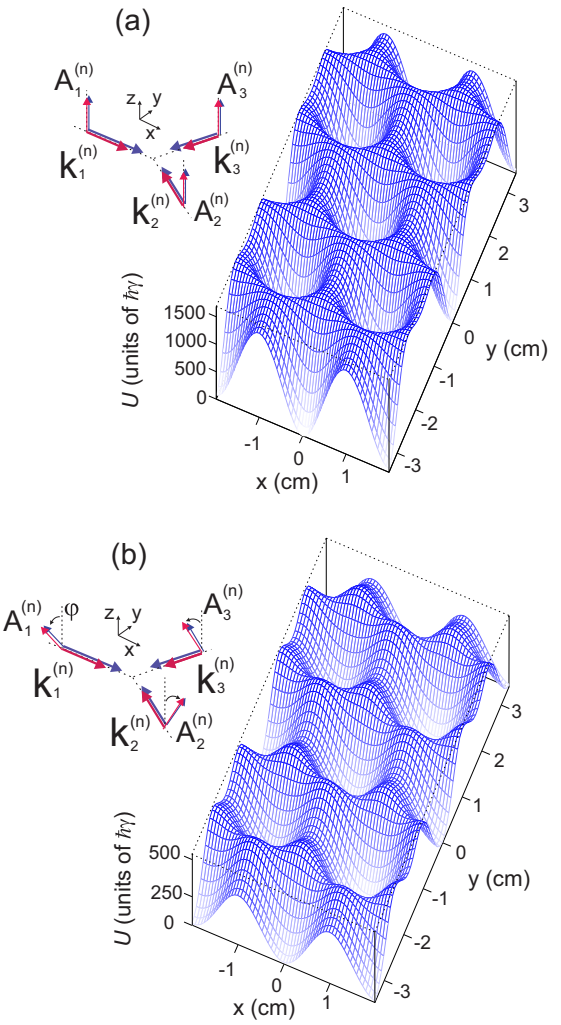

FIG. 12. (a) Macroscopic 2D optical potential formed by a bichromatic field of light waves with linear polarization along the z axis. The parameters of the waves correspond to the parameters of Figs. 3. (b) Macroscopic 2D optical potential generated by a bichromatic field of linearly polarized light waves oriented at an angle $\varphi = \pi/4$ to the z axis. The parameters of the waves correspond to the parameters of Fig. 9.

The presented deep macroscopic potentials can be used as an alternative to magnetooptical traps for the cooling and simultaneous trapping of lithium atoms. The number of atoms trapped from vapors can be estimated using the relation presented in [39,40]

$$N_c = \frac{L^2}{\sigma_c}\left(\frac{v_c}{u}\right)^4, \quad (52)$$

where v_c is the capture velocity, $u = (2k_BT/m)^{1/2}$ is the most probable speed, L is the size of the trap determined by the size of the laser beam, and σ_c is the cross section for an

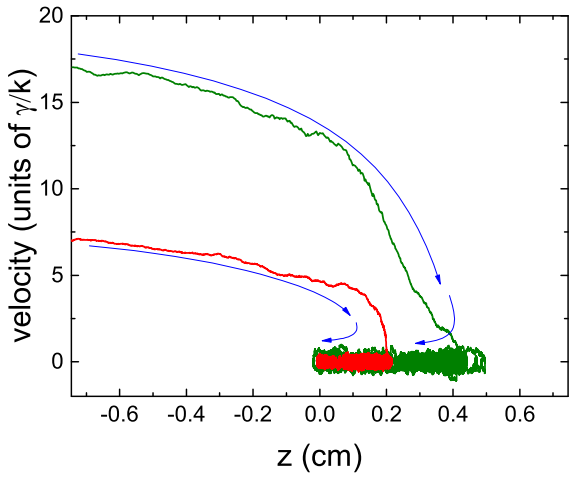

FIG. 13. The phase-space trajectory of an atom entering to the macroscopic trap formed by double lin ⊥ lin configuration of bichromatic field. The red (lower) line corresponds to atom trajectory in the trap with parameters of Fig. 9 ($\delta_1 = -1.5\gamma, \delta_2 = -\gamma, s_1 = 0.1, s_2 = 0.3$). The initial velocity of atoms on the trap boundary $v = 7\,\gamma/k \simeq 25$ m/s. The green (upper) line corresponds to the atom's trajectory in the trap with $\delta_1 = -10\gamma$, $\delta_2 = -2.5\gamma$, $s_1 = 0.05$, $s_2 = 0.5$. The initial velocity of atoms on the trap boundary $v = 17\,\gamma/k \simeq 60$ m/s. The blue arrows define the direction of the trajectory evolution.

atom to eject atom from a trap. The capture velocity can be found from the analysis of trajectories of atoms coming to the trap with different velocities, separating those that lead to the capturing of atoms. This analysis can be done on the basis of Langevin equations (see, for example, [13,41]) describing the atom trajectory under the light force and associated stochastic diffusion. Here we used numerical expressions for the force and diffusion as functions of velocity and the position of the atom. Figure 13 demonstrates the trajectory in the phase space of the atom captured in the macroscopic potential formed by the bichromatic field of the double lin ⊥ lin configuration. The direct numerical analysis results in $v_c \simeq 10\,k/\gamma \simeq 35$ m/s for the traps with parameters of Fig. 9, which leads to an estimation of $N_c \simeq 10^7$ for the number of trapped atoms. We additionally note that the number of trapped atoms N_c is determined not only by the capture velocity v_c, which can be increased by adjusting the parameters of the bichromatic field, but also by the most probable velocity at which atoms enter the trap u in (52). For lithium atoms loaded from vapors $u \simeq 900$ m/s (at temperature $T = 300$ K) is sufficiently large compared to the heavy elements (190 m/s for Cs atoms and 240 m/s for Rb atoms at temperature $T = 300$ K). Therefore, in many works, the methods of precooling and slowing down of atoms are used to increase the number of lithium atoms in MOT [42–44]. A similar technique can also be used to increase the number of atoms loaded into a bichromatic trap.

IV. CONCLUSION

In this paper, we present an idea of a deep pure-optical trap for neutral atoms based on a dissipative bichromatic optical lattice. For lithium atoms, as an example, a low-intensity bichromatic field (about 5 mW/cm^2) allows for the creation of a deep optical potential with a macroscopic period of centimeter scale, which provides laser cooling and trapping of atoms. The analysis, which was carried out within the one-atom approximation, showed that the temperature of laser cooling can reach values comparable to and below the Doppler limit (which is approximately $\simeq 140\,\mu$K for lithium atoms). At the same time, the localization of trapped atoms reaches submillimeter sizes and the number of trapped atoms is comparable to the number trapped in MOT.

It should also be noted that the presented idea of a deep dissipative lattice with a macroscopic period in a bichromatic field can be generalized to other neutral atoms. For example, for Rb and Cs atoms' transitions between hyperfine components of the D_2 line can be used as resonant transitions for two frequency components of the bichromatic lattice. In this case, the period of the macroscopic potential will be determined mainly by the splitting between the hyperfine components of the ground state $^2S_{1/2}$ and gives $\Lambda \simeq 4.9$ cm for ^{85}Rb, $\Lambda \simeq 2.2$ cm for ^{87}Rb, and $\Lambda \simeq 1.6$ cm for ^{133}Cs. Also, for odd isotopes of mercury atoms ^{199}Hg and ^{201}Hg, the intercombination transition $^1S_0 \to {}^3P_1$ ($\lambda = 253.7$ nm, $\gamma/2\pi = 1.3$ MHz) can be used, where the hyperfine splitting of the upper level $^3P_1$ exceeds 20 GHz that allows to create a bichromatic lattice with a macroscopic period of $\Lambda \simeq 0.7$ cm.

Such a deep pure-optical macroscopic potential can be used for the cooling and trapping of atoms in compact devices with low power consumption.

ACKNOWLEDGMENTS

We thank Ennio Arimondo for fruitful discussion and valuable comments. The research was supported by the Russian Science Foundation (Project No. 23-22-00198). The work of A.V.T. was supported by the Russian Science Foundation (Project No. 23-12-00182), and V.I.Y. was supported by the Ministry of Science and Higher Education of the Russian Federation (Project No. FSUS-2020-0036).

[1] E. Raab, M. Prentis, A. Cable, S. Chu, and D. Pritchard, Phys. Rev. Lett. **59**, 2631 (1987).
[2] H. J. Metcalf and P. V. D. Straten, *Laser Cooling and Trapping* (Springer, New York, 1999).
[3] P. R. Berman, *Atom Interferometry* (Academic, San Diego, 1997).
[4] M. Takamoto, I. Ushijima, N. Ohmae, T. Yahagi, K. Kokado, H. Shinkai, and H. Katori, Nat. Photon. **14**, 411 (2020).
[5] G. Lion, I. Panet, P. Wolf, C. Guerlin, S. Bize, and P. Delva, Journal of Geodesy **91**, 597 (2017).
[6] W. F. McGrew, X. Zhang, R. J. Fasano, S. A. Schäffer, K. Beloy, D. Nicolodi, R. C. Brown, N. Hinkley, G. Milani, M. Schioppo *et al.*, Nature (London) **564**, 87 (2018).
[7] T. Nicholson, S. Campbell, R. Hutson, B. Bloom, R. McNally, W. Zhang, M. Barret, M. Safronova, G. Strouse, W. Tew *et al.*, Nat. Commun. **6**, 6896 (2015).

[8] P. Jessen and I. Deutsch, Adv. At. Mol. Opt. Phys. **37**, 95 (1996).
[9] G. Grynberg and C. Robilliard, Phys. Rep. **355**, 335 (2001).
[10] J. Dalibard and C. Cohen-Tannoudji, J. Opt. Soc. Am. B **6**, 2023 (1989).
[11] K. Berg-Sørensen, Y. Castin, K. Mølmer, and J. Dalibard, Europhys. Lett. **22**, 663 (1993).
[12] O. N. Prudnikov, A. V. Taichenachev, A. V. Tumaikin, and V. I. Yudin, J. Exp. Theor. Phys. **104**, 839 (2007).
[13] O. N. Prudnikov and E. Arimondo, J. Opt. B: Quantum Semiclassical Opt. **6**, 336 (2004).
[14] J. Dalibard and C. Cohen-Tannoudji, J. Opt. Soc. Am. B **2**, 1707 (1985).
[15] O. N. Prudnikov, A. V. Taichenachev, A. M. Tumaikin, and V. I. Yudin, Phys. Rev. A **75**, 023413 (2007).
[16] O. N. Prudnikov, R. Y. Ilenkov, A. V. Taichenachev, A. M. Tumaikin, and V. I. Yudin, J. Exp. Theor. Phys. **112**, 939 (2011).
[17] A. P. Kulosa, D. Fim, K. H. Zipfel, S. Rühmann, S. Sauer, N. Jha, K. Gibble, W. Ertmer, E. M. Rasel, M. S. Safronova *et al.*, Phys. Rev. Lett. **115**, 240801 (2015).
[18] A. P. Kazantsev and I. V. Krasnov, JETP Lett. **46**, 332 (1987).
[19] V. S. Voitsekhovich, M. V. Danileiko, A. M. Negriiko, V. I. Romanenko, and Y. L. P., Zh. Tekh. Fiz. **58**, 1174 (1988).
[20] R. Grimm, Y. B. Ovchinnikov, A. I. Sidorov, and V. S. Letokhov, Phys. Rev. Lett. **65**, 1415 (1990).
[21] J. Söding, R. Grimm, Y. B. Ovchinnikov, P. Bouyer, and C. Salomon, Phys. Rev. Lett. **78**, 1420 (1997).
[22] M. T. Cashen and H. Metcalf, Phys. Rev. A **63**, 025406 (2001).
[23] T. C. Liebisch, E. Blanshan, E. A. Donley, and J. Kitching, Phys. Rev. A **85**, 013407 (2012).
[24] O. N. Prudnikov, A. S. Baklanov, A. V. Taichenachev, A. M. Tumaikin, and V. I. Yudin, J. Exp. Theor. Phys. **117**, 222 (2013).
[25] O. N. Prudnikov, A. V. Taichenachev, and V. I. Yudin, Quantum Electron. **47**, 438 (2017).
[26] V. K. Khersonskii, A. N. Moskalev, and D. A. Varshalovich, *Quantum Theory Of Angular Momentum* (World Scientific, Singapore, 1988).
[27] A. A. Kirpichnikova, O. N. Prudnikov, A. V. Taichenachev, and V. I. Yudin, Quantum Electron. **52**, 130 (2022).
[28] A. A. Kirpichnikova, O. N. Prudnikov, R. Y. Il'enkov, A. V. Taichenachev, and V. I. Yudin, Quantum Electron. **50**, 939 (2020).
[29] J. Dalibard and C. Cohen-Tannoudji, J. Phys. B: At. Mol. Phys. **18**, 1661 (1985).
[30] J. Javanainen, Phys. Rev. A **44**, 5857 (1991).
[31] O. N. Prudnikov, A. V. Taichenachev, A. M. Tumaikin, and V. I. Yudin, J. Exp. Theor. Phys. **88**, 433 (1999).
[32] A. V. Bezverbnyi, O. N. Prudnikov, A. V. Taichenachev, A. V. Tumaikin, and Y. V. I., J. Exp. Theor. Phys. **101**, 584 (2005).
[33] S. E. Hamann, D. L. Haycock, G. Klose, P. H. Pax, I. H. Deutsch, and P. S. Jessen, Phys. Rev. Lett. **80**, 4149 (1998).
[34] I. H. Deutsch and P. S. Jessen, Phys. Rev. A **57**, 1972 (1998).
[35] O. N. Prudnikov, A. V. Taichenachev, A. M. Tumaikin, and V. I. Yudin, J. Exp. Theor. Phys. **93**, 63 (2001).
[36] O. N. Prudnikov, A. V. Taichenachev, A. M. Tumaikin, and V. I. Yudin, Jetp Lett. **70**, 443 (1999).
[37] E. Kalganova, O. Prudnikov, G. Vishnyakova, A. Golovizin, D. Tregubov, D. Sukachev, K. Khabarova, V. Sorokin, and N. Kolachevsky, Phys. Rev. A **96**, 033418 (2017).
[38] A. Hemmerich and T. W. Hänsch, Phys. Rev. Lett. **70**, 410 (1993).
[39] C. Monroe, W. Swann, H. Robinson, and C. Wieman, Phys. Rev. Lett. **65**, 1571 (1990).
[40] K. E. Gibble, S. Kasapi, and S. Chu, Opt. Lett. **17**, 526 (1992).
[41] J. Javanainen, Phys. Rev. A **46**, 5819 (1992).
[42] U. Schünemann, H. Engler, M. Zielonkowski, M. Weidemüller, and R. Grimm, Opt. Commun. **158**, 263 (1998).
[43] R. Hulet, J. H. V. Nguyen, and R. Senaratne, Rev. Sci. Instrum. **91**, 011101 (2020).
[44] D. Hernandez-Rajkov, J. E. Padilla-Castillo, M. Mendoza-Lopez, R. Colin-Rodriguez, A. Gutierrez-Valdes, S. A. Morales-Ramirez, R. A. Gutierrez-Arenas, C. A. Gardea-Flores, R. Jauregui-Renaud, J. A. Seman *et al.*, Rev. Mex. Fís. **66**, 388 (2020).